Probiotics and Antimicrobial Proteins
https://doi.org/10.1007/s12602-025-10874-y

RESEARCH

Multicopy Expression of the Marine Antimicrobial Peptide Spgillcin$_{177–189}$ in *Pichia pastoris* for High-Yield Production and Potent Activity Against Foodborne Pathogens

Xianxian Dong[1] · Huiliang Liao[1] · Chang Zhang[1] · Fangyi Chen[1,2,3] · Hui Peng[1,2,3] · Xiao Hong[1,2,3] · Hua Hao[1,2,3] · Ming Xiong[1,2,3] · Jiahao Ma[4] · Ke-jian Wang[1,2,3]

Received: 27 August 2025 / Accepted: 30 November 2025
© The Author(s), under exclusive licence to Springer Science+Business Media, LLC, part of Springer Nature 2025

Abstract

Bacterial foodborne contamination poses a dual challenge of chemical preservative risks and antibiotic resistance, drives the need for green production of natural antimicrobial alternatives. The reported cationic antimicrobial peptide (AMP) Spgillcin$_{177–189}$ derived from the *Scylla paramamosain*, has strong antimicrobial activity against S*taphylococcus aureus* and clinical isolation strains. To meet industry demand in future, large-scale production of Spgillcin$_{177–189}$ is essential. In the study, *Pichia pastoris* expression system was established for production of the recombinant Spgillcin$_{177–189}$ (rSpgillcin$_{177–189}$). Then, multicopy strategy was selectively designed by employing the Golden Gate assembly technology to efficiently construct multi-copy plasmids, which significantly enhanced the expression level of Spgillcin$_{177–189}$. A yield of 126.1 mg/L was harvested with 2.75-fold higher that of the single-copy strain. In addition, the recombinant Spgillcin$_{177–189}$ exhibited potent antibacterial activity against multiple foodborne pathogens within a MIC range of 5.25–84 μg/mL. It also showed effective bactericidal activity and anti-biofilm activity against S*taphylococcus aureus* and *Vibrio parahaemolyticus*. rSpgillcin$_{177–189}$ exhibited good thermostability, with no obvious cytotoxicity and hemolytic activity. rSpgillcin$_{177–189}$ may interact with microbial surface components via hydrogen bonding, which were vital for peptide activity in combating bacteria. The rSpgillcin$_{177–189}$ specifically targeting the cell membrane, disrupted bacterial membrane integrity and leading to cell death. This study provided a very feasible genetic engineering strategy for large-scale production of rSpgillcin$_{177–189}$, which will be applied at a lower cost in agricultural and food industries in future.

Keywords Pichia pastoris · Gene dosage · Antimicrobial peptide · Spgillcin$_{177-189}$ · Antimicrobial activity · Foodborne pathogen control

Introduction

Foodborne pathogens, including S*taphylococcus aureus* (*S. aureus*), *Bacillus cereus* (*B. cereus*), *Listeria monocytogenes* (*L. monocytogenes*) and *Vibrio spp*., pose a significant threat to human health, and the resulting foodborne illnesses have emerged as a critical public health concern worldwide [1]. Surveillance data indicates that 31 known foodborne pathogens account for an annual disease burden of over 9.4 million cases in America, including 55,961 hospital admissions and 1,351 fatalities [2]. Also, the misutilization and overutilization of antibiotics in both medical and agricultural fields have significantly accelerated the appearance of foodborne multidrug-resistant pathogens and dissemination of antibiotic resistance, which has become one of the

✉ Fangyi Chen
chenfangyi@xmu.edu.cn

✉ Ke-jian Wang
wkjian@xmu.edu.cn

1 State Key Laboratory of Marine Environmental Science, College of Ocean & Earth Sciences, Xiamen University, Xiamen, Fujian, China

2 State-Province Joint Engineering Laboratory of Marine Bioproducts and Technology, College of Ocean & Earth Sciences, Xiamen University, Xiamen, Fujian, China

3 Marine Biological Antimicrobial Peptide Industry Research Institute, Fujian Ocean Innovation Center, Xiamen 361102, China

4 Guangzhou Liyang Aquatic Technology Co., Ltd, Guangzhou, Guangdong, China

Published online: 15 December 2025

greatest threats to global health [3, 4]. Therefore, there is as an urgent need to develop novel natural antimicrobial agents that possess both high antibacterial efficacy and a low propensity to induce resistance, in order to control foodborne pathogens and mitigate the threat of foodborne multi-drug resistant pathogens to global health.

As integral components of innate immunity, antimicrobial peptides (AMPs) are the first line of defense against pathogens and are considered promising alternatives to conventional antibiotics [5]. Their importance is magnified in species such as *Scylla paramamosain*, which rely solely on innate immunity. Their multiple molting cycles and temporary fasting periods increase susceptibility to pathogens [6], and may have evolved a rich repertoire of AMPs, making it a valuable resource for novel AMP discovery. In our previous study, Spgillcin$_{177-189}$, a chemically synthesized truncated peptide identified from *Scylla paramamosain*, exhibited potent antimicrobial activity against *S. aureus*, *Pseudomonas aeruginosa* (*P. aeruginosa*) at a minimum inhibitory concentrations (MIC) range of 10.5–42 μg/mL. And drug-resistance assays showed that clinically drug-resistant strains *S. aureus* and *P. aeruginosa* failed to develop resistance to Spgillcin$_{177-189}$ after 50 days of continuous exposure, whereas conventional antibiotics such as rifampicin produce a significantly resistance at the 28th day, suggesting that the resistance-inducing tendency of Spgillcin$_{177-189}$ is low [7]. These findings confirm Spgillcin$_{177-189}$ as a novel antimicrobial agent, with substantial potential for industrial applications. However, the chemical synthesis of AMPs is costly and complex, greatly limiting their applications in the agriculture and food industries [8, 9]. In contrast, recombinant expression systems provide a cost-effective and scalable alternative for AMP production [10].

Recombinant expression systems commonly used for antimicrobial peptide (AMP) production include *Escherichia coli* (*E. coli*), yeast, and mammalian cell expression systems [11]. Among them, *E. coli* is the most widely used host; however, AMP expression in *E. coli* is often limited by peptide cytotoxicity and degradation by endogenous proteases, resulting in low yield and stability [12]. Mammalian systems can efficiently secrete proteins but are constrained by slow growth and high production costs, which limit their industrial applicability [11]. In contrast, the eukaryotic yeast *Pichia pastoris* (*P. pastoris*) has emerged as an attractive host owing to its genetic stability, strong secretion capacity, and suitability for high-density fermentation [13]. Importantly, *P. pastoris* allows for more accurate translation and post-translational modification of target proteins, which are critical for maintaining the bioactivity of recombinant proteins [14], making it the best choice for the synthesis of Spgillcin$_{177-189}$. However, the yield of recombinant proteins in *P. pastoris* is highly variable, and efficient expression of all proteins cannot be guaranteed [15–17]. To enhance expression efficiency, several strategies have been employed, including codon optimization [18], signal peptide engineering [19], promoter engineering [20], optimizing gene dosage, and co-expression of chaperone proteins [21]. Among them, the multicopy strategy remains one of the most effective approaches. This study employed rationally designed multicopy plasmids rather than random genomic integration for strain construction. This strategy allows precise control of gene copy number, significantly streamlines the strain development process, and ensures reliable and scalable expression of the recombinant peptide in *P. pastoris*.

In this study, we aimed to establish an efficient *P. pastoris* expression system for the large-scale production of rSpgillcin$_{177-189}$ to facilitate its practical development. To overcome production limitations, a multicopy expression strategy coupled with high-density fermentation was employed. Furthermore, the rSpgillcin$_{177-189}$ was purified by cation-exchange chromatography, and its antimicrobial properties and potential mechanisms of action were systematically evaluated. This work provides a theoretical and technical basis for the sustainable production and potential application of rSpgillcin$_{177-189}$ in the food industries.

Materials and Methods

Peptide Information, Strain, Plasmid, and Cultivation Conditions

Spgillcin$_{177-189}$, a cationic AMP identified from *S. paramamosain* with the sequence KKRRCFFRHIYVA. This chemically synthesized truncated peptide features a molecular weight of 1.7 kDa, a net charge of + 5 and a hydrophobicity of 34%.

E. coli DH5α and DH10β were purchased from Invitrogen (California, USA) for plasmid construction. *P. pastoris* GS115, the plasmids pPIC9 (GenBank: Z46233.1), pPIC9k (GenBank: Z46234.1), and pPICZαA (https://www.genscript.com/vertor/library_list) were purchased from Invitrogen (California, USA). *E. coli* DH5α and *P. pastoris* GS115 was cultured in LB medium (10 g/L tryptone, 5 g/L yeast extract, 10 g/L NaCl) and Yeast extract peptone dextrose medium (YPD) (20 g/L tryptone, 10 g/L yeast extract, 10 g/L glucose), respectively, and antibiotics (ampicillin 100 μg/mL, zeocin 100 μg/mL, kanamycin 50 μg/mL) were added as necessary. Buffered glycerol-complex medium (BGMY) (100 mM potassium phosphate, 10 g/L glycerol, 10 g/L yeast extract, 20 g/L peptone, 13.4 g/L Yeast Nitrogen Base (YNB), 0.4 mg/L biotin) and Buffered methanol-complex medium (BMMY) (100 mM potassium phosphate, 5 mL/L

glycerol, 10 g/L yeast extract, 20 g/L peptone, 13.4 g/L YNB, 0.4 mg/L biotin) were used for shake flask fermentation.

The standard strains were purchased from the China General Microorganism Culture Collection Center (CGMCC), including *B. cereus* (CGMCC No. 1.3760), *L. monocytogenes* (CGMCC No. 1.10753), *Staphylococcus epidermidis* (CGMCC No. 1.4260), *S. aureus* (CGMCC No. 1.2465), *Acinetobacter baumannii* (CGMCC No. 1.6769), *Pseudomonas aeruginosa* (CGMCC No. 1.2421), *Vibrio fluvialis* (CGMCC No. 1.1609), *Vibrio harveyi* (CGMCC No. 1.1593), *Vibrio alginolyticus* (CGMCC No. 1.1833), *V. parahaemolyticus* (CGMCC No. 1.1615).

The clinical strains obtained from the Second Affiliated Hospital of Fujian Medical University, including MDR *A. baumannii* QZ18050, MDR *A. baumannii* QZ18055, MDR *P. aeruginosa* QZ19121, MDR *P. aeruginosa* QZ19122, MRSA QZ19130.

Mouse macrophages (RAW264.7) cell came from National Infrastructure of Cell Line Resource (Beijing, China). Human embryonic kidney cells (HEK-293T) sourced from Stem Cell Bank at the Chinese Academy of Sciences (Shanghai, China). Zebrafish embryonic cell line (ZF4) was obtained from Institute of Hydrobiology (Wuhan, China).

Plasmids and Strain Construction

The *Spgillcin*$_{177-189}$ (*Spg*) sequence was optimized by GenScript Biotech Corporation (Nanjing, China). The optimized sequence was then inserted into the pPIC9 vector using *Xho* I and *Not* I restriction enzymes, to obtain the recombinant plasmid pPIC9-*Spg*. Subsequently, the pPIC9-*Spg* that linearized using *Sal* I was transformed into *P. pastoris* GS115 via electroporation. The transformed cells were cultured on Minimal Dextrose Medium (MD) plates at 28℃ for 3 days to screen for positive clones.

Construction of Multicopy Backbone Plasmid and Multiple Copy Spg Expression Vectors

All the primers used to construct the backbone plasmid pHC were listed in Table S1, and the fragments were assembled using the Gibson assembly method. The construction workflow of the backbone plasmid pHC was illustrated in Fig. 2a. Briefly, the Cre recombinase fragment was synthesized by overlap PCR in vitro and inserted into the pPICZαA plasmid to generate pPICZ-Cre. The recombinant plasmid, pPICZ-cre-lox, was obtained using overlap extension PCR with the addition of the lox71 and lox66 sites at the end of the Cre cassette and the BleoR fragment, respectively. Subsequently, PCR amplified HIS4 gene from pPIC9 and cloned into pPICZ-cre-lox to obtain the final plasmid, pHC-AOX.

Multi-copy plasmids were then constructed via the Golden Gate assembly method. Primers with *Bsa* I restriction sites were designed for amplification of the *Spg* expression cassettes through the NEB website (https://goldengate.neb.com/#!/). Multiple fragments were ligated into the backbone plasmid pHC and transformed into *E. coli* DH10β. The resulting recombinant multi-copy plasmids were named pHC-spg-2c, pHC-spg-3c, pHC-spg-4c, pHC-spg-5c, and pHC-spg-6c. Subsequently, the multi-copy plasmids that linearized by *Sal* I or *Hpa* I were transformed into *P. pastoris* GS115 via electroporation. The transformed cells were cultured on YPD-zeocin plates at 28℃ to select positive transformants.

Inducible Expression of rSpgillcin$_{177-189}$

To induce expression of the target peptide, transformants were inoculated in YPD or YPDZ medium at 28℃ overnight. Then, it was inoculated into BMGY medium with 1% inoculum and cultured at 28 °C for 24 h. When the OD_{600} reached 2–10, the culture was collected by centrifugation (2000 g, 10 min) and adjusted to an initial optical density (OD_{600}) of 1.0 in BMMY medium prior to expression induction. Methanol was added to induce expression every 24 h to a final concentration of 0.5%. The expression level of rSpgillcin$_{177-189}$ was identified using Tricine SDS-PAGE, and the gray scale of the target bands was quantified using Image J software (NIH, USA) to estimate the relative expression of the peptide in all samples.

High-Density Fermentation

For large-scale production of rSpgillcin$_{177-189}$, high-density fermentation was performed in a 50 L fermenter. The selected transformants were inoculated into 20 mL YPD medium in a shaking flask and cultured at 30 °C at 200 rpm for 22 h. The seed culture was then inoculated to 400 mL of YPD medium and incubated for 8 h. Subsequently, the seed culture was inoculated into fermenter containing 12 L of BSM medium. During fermentation, the pH and temperature were maintained at 5.5 and 28 °C, respectively, with a stirring speed of 200–700 rpm and an airflow rate of 1.4 v/min. Methanol was added to induce expression when the wet cell weight (WCW) reached 200 g/L, and dissolved oxygen was controlled at approximately 20%. Samples were collected throughout the fermentation to measure wet cell weight. Finally, the recombinant peptide expression level was assessed by Tricine-SDS-PAGE. The yield of rSpgillcin$_{177-189}$ was quantified using Image J software as previously described, with the synthetic peptide serving as a standard.

Purification of rSpgillcin$_{177-189}$ by Ion-Exchange Chromatography

For purification of rSpgillcin$_{177-189}$, the fermentation supernatant was collected by centrifugation. The supernatant was dialyzed against the binding buffer (100 mM sodium phosphate buffer, pH 6.0) at 4°C for 5 h, and repeated three times. The dialyzed supernatant was loaded onto a Capto™ SP ImpRes cation exchange column (Cytiva, America). Subsequently, the column was pre-equilibrated with binding buffer at a 0.5 mL/min flow rate. The AKTA system (GE, USA) was used to purify the peptide via linear gradient elution (0–500 mM NaCl) in elution buffer (100 mM PBS, 1 M NaCl, pH 6.0) at a constant flow rate of 1 mL/min. After purification, the column was equilibrated and stored in storage buffer (200 mM NaAc containing 20% ethanol) at 4°C. The purified samples were dialyzed against ultrapure water for desalting, followed by freeze-drying. The resulting peptide powder was stored at − 80 °C until further use.

Antimicrobial Assay

To identify the biological activity of rSpgillcin$_{177-189}$, the antimicrobial activity of rSpgillcin$_{177-189}$ was determined as previous study [22]. Briefly, bacterial suspensions in the logarithmic growth phase were diluted to 10^6 CFU/mL in MH medium and inoculated into 96-well plates. Different concentrations of rSpgillcin$_{177–189}$ (5.25–84 μg/mL) were diluted with sterile water. Then, the peptide solution and bacterial suspensions were mixed thoroughly, and cultured at 37°C and 28°C for 24 h. Each well contained a final volume of 100 μL, consisting of 50 μL of bacterial suspension and 50 μL of rSpgillcin$_{177–189}$ solution. Milli-Q water was used as a control. The lowest peptide concentration with no visible bacterial growth was defined as the MIC; the lowest concentration that killed 99.99% of bacteria was recorded as the minimum bactericidal concentration (MBC). Antimicrobial assays were performed three times.

Time-Killing Kinetics Assay

Time-killing kinetics assays were conducted to evaluate the bactericidal activity of rSpgillcin$_{177-189}$ against *S. aureus* and *V. parahaemolyticus*. Briefly, bacterial cultures in the exponential growth phase were adjusted to approximately 1×10^5 CFU/mL and mixed with an equal volume of rSpgillcin$_{177-189}$ at 1×MIC. The mixtures were incubated at 37°C and 28°C, respectively, and aliquots were removed at designated time points for viable cell enumeration by plate counting. Each assay was performed in triplicate and independently repeated three times.

Biofilm Formation Inhibition and Mature Biofilm Disruption Assay

The effect of rSpgillcin$_{177-189}$ on biofilm formation was assessed using the crystal violet method. Briefly, bacterial cultures at the logarithmic growth phase were adjusted to 1×10^6 CFU/mL for *S. aureus* and 1×10^5 CFU/mL for *V. parahaemolyticus*. The suspensions were incubated with varying concentrations of rSpgillcin$_{177-189}$ (0–84 μg/mL) for 24 h. Following incubation, planktonic cells were removed, and the attached biofilms were stained with 0.1% crystal violet. Absorbance was subsequently quantified at 595 nm using a microplate reader (BioTek, USA).

Similarly, the eradication activity of rSpgillcin$_{177-189}$ against mature biofilms was evaluated. Bacterial suspensions were diluted to 1×10^5 CFU/mL and incubated for 24 h to allow biofilm maturation. After removal of the supernatant, fresh medium containing rSpgillcin$_{177-189}$ (0–84 μg/mL) was added and further incubated for 24 h. The biofilms were then stained with 0.1% crystal violet as described above, and absorbance was measured at 595 nm. The experiment was performed in triplicate and repeated three times.

SEM and TEM Analysis

Following previous methodologies, SEM was utilized to examine the effects of rSpgillcin$_{177-189}$ on *S. aureus* and *V. parahaemolyticus* [23]. In this procedure, log-phase bacterial cultures of *S. aureus* and *V. parahaemolyticus* were first collected and diluted with PBS to 1×10^7 cfu/mL. The bacterial suspension was then incubated with rSpgillcin$_{177-189}$ for 30 min. Subsequently, the treated samples were fixed with 2.5% glutaraldehyde at 4 °C for 120 min, rinsed with PBS, and deposited onto glass slides. Next, the cells were graded ethanol dehydration, and then dried in a critical point dryer (Leica, Germany). Finally, the samples were gold-coated and observed using a scanning electron microscope (Thermo Fisher, USA).

TEM analysis was performed following a previously established protocol [6]. Briefly, *S. aureus* and *V. parahaemolyticus* were treated with rSpgillcin$_{177-189}$ at 37 °C and 28 °C for 30 min. After incubation, the cells were embedded in 2% agarose. Subsequently, the samples were fixed with 2.5% glutaraldehyde and incubated at 4 °C for 12 h. After fixation, the samples were washed with PBS, and post-fixed with 1% osmium tetroxide. The specimens were subjected to graded dehydration and rinsing, then the samples were embedded using epoxy resin. Finally, ultrathin sections were prepared and examined using a transmission electron microscope (HT7800, Hitachi, Japan).

Membrane Permeability Assay

The effect of rSpgillcin$_{177-189}$ on bacterial membrane permeability was evaluated using the LIVE/DEAD BacLight™ Bacterial Viability Kit (Thermo Fisher, USA). *S. aureus* and *V. parahaemolyticus* were diluted to 1×10^7 CFU/mL with PBS and incubated with rSpgillcin at 1 × MIC, with LL-37 as a positive control. Following incubation, the cells were washed twice with PBS and resuspended in a SYTO9/PI dye mixture for fluorescence staining. Fluorescence images were then captured using a confocal laser scanning microscope (CLSM) (Zeiss LSM780, Germany).

Microbial Surface Components Binding Assays

The binding of rSpgillcin$_{177-189}$ to LPS or LTA was assessed following previously described methods. Briefly, 25 µL of rSpgillcin$_{177-189}$ at a final concentration of 1×MBC (21 and 42 µg/mL) was mixed with 25 µL of LPS or LTA (8 to 64 µg/mL) in 96-well plate. Subsequently, 50 µL of bacterial suspension containing *S. aureus* or *V. parahaemolyticus* (1×10^6 CFU/mL) was added to each well. Absorbance was measured at 600 nm using a microplate reader (BioTek, USA). The experiment was performed in triplicate and repeated three times.

HPLC and LC-MS Analysis

The purity of rSpgillcin$_{177-189}$ was determined by analytical high-performance liquid chromatography (HPLC). The peptide was diluted to a final concentration of 0.1 mg/mL with ultrapure water for analysis. HPLC was performed using a C18 reversed-phase column (Agilent, America) with a mobile phase of ultrapure water (solvent A) and acetonitrile (solvent B). The peptide was eluted using a linear gradient of 5–95% acetonitrile at a flow rate of 1.0 mL/min, with UV detection at 220 nm. The peptide purity was calculated based on the relative peak area.

LC-MS analysis was used to verify the molecular mass and integrity of the rSpgillcin$_{177-189}$. Briefly, the purified rSpgillcin$_{177-189}$ was dissolved and adjusted to a concentration of 0.1 mg/mL in ultrapure water, and then analyzed using Thermo Orbitrap Fusion Lumos mass spectrometer (Thermo Scientific, America). The raw data were processed with Proteome discover software, and spectra were aligned against the target sequence database for final identification.

Circular Dichroism (CD) Spectroscopy

CD spectroscopy was used for determining the secondary structure of the rSpgillcin$_{177-189}$ in a JascoJ-715 spectrophotometer (Jasco, Japan). The rSpgillcin$_{177-189}$ was dissolved in ddH_2O or 60 mM SDS or 50% trifluoroethanol (TFE) with a final 0.2 mg/mL. The spectra of the samples were scanned from 190 to 260 nm with a scanning speed of 100 nm/min at 25°C. The other scan parameters were set to 0.1 cm path length and 2 nm bandwidth. The secondary structure of rSpgillcin$_{177-189}$ was analyzed using CDNN software.

Molecular Docking

The 3D structure of Spgillcin$_{177-189}$ was predicted by the PEP-FOLD3 server. Molecular docking with the ligands LTA and LPS was conducted using Autodock Vina following a reported method [24]. Prior to docking, all structures were preprocessed in Autodock Tool by adding charges and hydrogens. The parametric dimension values of the grid box were adjusted to X = 53.49, Y = 71.64, Z = 54.44 (for LPS) and X = 9.46, Y = 18.51, Z = −14.49 (for LTA) to center on the putative binding sites. Semi-flexible docking was performed, and the output poses were analyzed using Pymol 3.0.0 software.

Thermostability Assays

The stability of rSpgillcin$_{177-189}$ was assessed following a previously established method with minor modifications [25]. Briefly, *S. aureus* and *V. parahaemolyticus* were diluted to 1×10^6 CFU/mL during the logarithmic growth phase. For thermal stability assessment, rSpgillcin$_{177-189}$ was incubated at 100°C for various time (10, 20, and 30 min), or at different temperatures (16, 28, 37, 60, 80, 121°C) for 25 min, respectively, and followed by rapid cooling to room temperature. The heat-treated rSpgillcin$_{177-189}$ solutions were then mixed with the bacterial suspensions in 96-well plates and cultured at 37 °C for 24 h. All experiments were performed in triplicate and repeated three times.

Cytotoxicity and Hemolytic Activity

The cytotoxicity of rSpgillcin$_{177-189}$ toward mammalian cells was examined using the MTT-PMS method. Briefly, HEK293T, RAW264.7, and ZF4 cells were adjusted to 1×10^5 cells/mL and cultured overnight in 5% CO_2 incubators at 37°C and 28°C, respectively. After removing the medium, fresh medium containing different concentrations of rSpgillcin$_{177-189}$ was added and incubated overnight. Cell viability was subsequently determined by measuring absorbance at 492 nm using a microplate reader (BioTek, USA).

The hemolytic activity of rSpgillcin$_{177-189}$ was evaluated using mouse erythrocytes as described previously [26]. Briefly, mouse erythrocytes were collected and diluted with 0.9% saline to 0.4% (v/v). The erythrocyte suspension was

mixed with various concentrations of rSpgillcin$_{177–189}$ (5.25, 10.5, 21, 42, and 84 μg/mL) and incubated at 37 °C for 1 h. Saline and 1% Triton X-100 served as negative and positive controls, respectively. The mixtures were centrifuged at 1500 g for 5 min, and the absorbance of the supernatants was measured at 540 nm. All experiments were performed in triplicate and repeated three times.

qPCR

To quantify the copy number of the *spg* gene, genomic DNA was extracted from multi-copy *P. pastoris* strains using a Yeast Genomic DNA Isolation Kit (Solarbio, Beijing, China). qPCR was performed with genomic DNA as the template, following the instructions provided by the manufacturer (Takara, Dalian, China), and qCPR primers were listed in Table S1. The copy number of the *spg* gene was determined using the $2^{-\Delta\Delta CT}$ method, with ACT1 (Gene ID: 8200200) serving as the reference gene.

Statistical Analysis

GraphPad 9.0, R Studio 3.4.6, and Image J software were used for plotting and statistical analysis. All experiments were independently conducted in triplicate, and the results are shown as mean ± SD. Statistical significance was determined using one-way ANOVA with a threshold of $p < 0.05$.

Results

Plasmid Construction and Recombinant Expression of rSpgillcin$_{177-189}$

The construction of the recombinant plasmid is illustrated in Fig. 1a. In brief, the Spgillcin$_{177-189}$ gene sequence was inserted after the α-factor signal peptide of pPIC9, generating the Spgillcin$_{177-189}$ cassette, which was named pPIC9-*spg*. Then, the positive transformants were selected for inducible expression. Supernatants from fermentation were collected at various time points (24, 48, 72, and 96 h), and the results were shown in Fig. 1b. The theoretical molecular weight of Spgillcin$_{177-189}$ is 1.7 kDa; however, Tricine-SDS-PAGE analysis revealed an actual molecular weight ranging from 1.7 to 4.6 kDa. The discrepancy between the apparent molecular weight on Tricine–SDS–PAGE and the theoretical value can be attributed to the physicochemical properties of rSpgillcin$_{177–189}$. Because rSpgillcin$_{177–189}$ (sequence: KKRRCFFRHIYVA) is a short, cationic peptide rich in polar and hydrophobic residues, its mobility on Tricine-SDS-PAGE would be affected by polar amino acids, so its apparent molecular weights had a distance from their

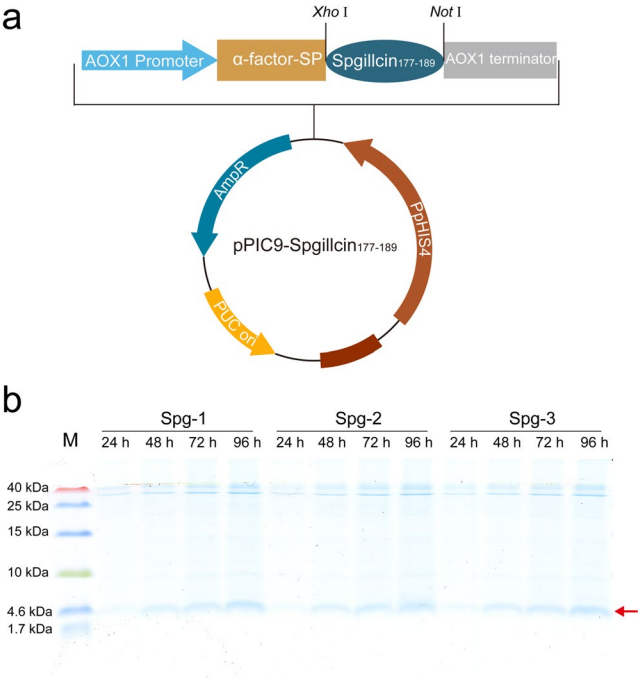

Fig. 1 Vector construction and recombinant proteins expression. (**a**) Schematic diagram of recombinant expression vector pPIC9-Spgillcin$_{177-189}$. (**b**) Tricine-SDS-PAGE analysis of rSpgillcin$_{177-189}$ at different times

theoretical molecular weights, this phenomenon was found in previous studies, AMPs exhibit a slower migration rate in Tricine-SDS-PAGE and have an apparent molecular weight that is relatively larger [27–29].

Construction of Multicopy Backbone Plasmid pHC and *Spg* Multicopy Plasmid

To simplify the construction of multicopy plasmids, the pHC multi-copy backbone plasmid was constructed using the pPICZαA plasmid as a scaffold (Fig. 2a). The MCS region of the pHC plasmid, including the *Not* I, *EcoR* I, and two *Bsa* I sites, which are used for constructing multi-copy plasmids and restriction enzyme digestion detection. As illustrated in Fig. 2b, Golden Gate assembly technology was employed to construct multi-copy plasmids, including pHC-spg-1c, pHC-spg-2c, pHC-spg-3c, pHC-spg-4c, pHC-spg-5c, and pHC-spg-6c, each harboring 1, 2, 3, 4, 5, or 6 copies of the *Spg* gene, respectively. All recombinant plasmids were verified by Sanger sequencing and Keseq sequencing to ensure the integrity and accuracy of the inserted sequences.

Effect of Multicopy Strategy on the Expression Level of rSpgillcin$_{177-189}$

Positive transformants contained various copies *spg* gene were selected for inducing expression and analyzing the copy

number. The copy number analysis of *spg* gene is shown in Table 1, consistent with the theoretical copy number. Then, the expression levels of various transformants were determined by Tricine-SDS-PAGE, the results were shown in Fig. 2e. Tricine-SDS-PAGE displayed a prominent band at 1.7–4.6 kDa, corresponding to the target peptide. The highest expression level of rSpgillcin$_{177-189}$ was observed in the 4-copy strain (Fig. 2c). Gray-scale analysis revealed that the rSpgillcin$_{177-189}$ expression level in the GS115-pHC-spg-4c strain was 2.75-fold higher than that in the single-copy strain (Fig. 2d), reaching 13.4 mg/L. These results indicated that the multicopy integration strategy significantly enhances the expression level of rSpgillcin$_{177-189}$.

High-Density Fermentation and Purification of rSpgillcin$_{177-189}$

In this study, high-density fermentation was performed using glycerol as the initial carbon source, with the entire fermentation process illustrated in Fig. 3a. Methanol induction was initiated at 27 h, and as the cells gradually adapted to the methanol-based carbon source, both cell wet weight and the expression level of the rSpgillcin$_{177-189}$ exhibited a progressively increase (Fig. 3b, c). In this study, the concentration of rSpgillcin$_{177-189}$ in the fermentation supernatant reached a peak of 121.6 mg/L at 48 h (Fig. 3c, d). The rSpgillcin$_{177-189}$ was isolated and purified using cation exchange chromatography. The purified rSpgillcin$_{177-189}$ was obtained with a high purity of >95%, as assessed by both Tricine-SDS-PAGE and HPLC (Fig. 3c, Fig. S1). The molecular mass and integrity of the rSpgillcin$_{177-189}$, were verified by LC-MS (Fig. S2). The analysis revealed 100% sequence coverage, confirming that the peptide secreted and expressed by *P. pastoris* matches the designed theoretical sequences. Subsequently, purified rSpgillcin$_{177-189}$ was lyophilized and stored at −80 °C for further analysis.

Antimicrobial Activity of rSpgillcin$_{177-189}$

The antimicrobial activity of rSpgillcin$_{177-189}$ is shown in Table 3. We first evaluated the antimicrobial activity of rSpgillcin$_{177-189}$ against *S. epidermidis*, *S. aureus*, *(A) baumannii*, *P. aeruginosa*, and clinical multidrug-resistant (MDR) strains (*P. aeruginosa* and MRSA). The results were consistent with previous findings, showing MIC values ranging from 5.25 to 42 μg/mL and MBC values below 84 μg/mL. Moreover, we further assessed its antimicrobial activity against foodborne pathogens, including *Vibrio spp*., (*V. fluvialis*, *V. harveyi*, *V. alginolyticus*, and *V. parahaemolyticus*), *(B) cereus* and *L. monocytogenes*. rSpgillcin$_{177-189}$ exhibited potent antimicrobial activity against these foodborne pathogens, with MIC values between 5.25 and 42 μg/mL and MBC values lower than 84 μg/mL. These results indicated that it had broad-spectrum antimicrobial activity against foodborne pathogens. *S. aureus* and *V. parahaemolyticus* are among the most prevalent foodborne pathogens responsible for food poisoning and acute gastroenteritis. Severe infections may progress to septicemia, thereby representing a significant threat to public health. Therefore, we chose these two strains as the test bacteria for the following experiments.

Killing Kinetic of rSpgillcin$_{177-189}$

The bactericidal efficiency of rSpgillcin$_{177-189}$ was assessed by bactericidal kinetics. As shown in Fig. 4a & b, rSpgillcin$_{177-189}$ at 1×MIC killed 99.9% of *S. aureus and V. parahaemolyticus* in 30–90 min, respectively.

Effect of rSpgillcin$_{177-189}$ on Bacteria Morphological Change

The effects of rSpgillcin$_{177-189}$ on morphological changes in *S. aureus* and *V. parahaemolyticus* were observed using SEM and TEM. As shown in Fig. 4c & d, PBS-treated *S. aureus* and *V. parahaemolyticus* exhibited normal morphology and smooth surfaces. In contrast, after rSpgillcin$_{177-189}$ treatment, *S. aureus and V. parahaemolyticus* exhibited noticeable wrinkling, and the integrity of the bacterial cell membranes was disrupted, ultimately leading to the leakage of intracellular contents.

Anti-Biofilm Activity of rSpgillcin$_{177-189}$

The inhibitory effect of rSpgillcin$_{177-189}$ on biofilm formation of *S. aureus and V. parahaemolyticus* was evaluated. The results demonstrated that rSpgillcin$_{177-189}$ attenuated the ability of biofilm formation in both strains in a dose-dependent manner. When the concentration reached 84 μg/mL, the inhibition rates of biofilm formation reached 75% and 90.1% against *V. parahaemolyticus and S. aureus*, respectively (Fig. 5a, c).

The efficacy of rSpgillcin$_{177-189}$ in eliminating mature biofilm was evaluated. At a concentration of 84 μg/mL, rSpgillcin$_{177-189}$ eradicated mature biofilms of *V. parahaemolyticus* and *S. aureus* with elimination rates of 82.9% and 85.4%, respectively (Fig. 5b, d). These findings indicate that rSpgillcin$_{177-189}$ exhibits potent antibiofilm activity against both pathogens.

Effect of rSpgillcin$_{177-189}$ on Membrane Permeability

Bacterial membrane permeability was assessed using SYTO9 and PI staining. SYTO9 labels all bacterial cells, whereas PI selectively penetrates and stains cells with

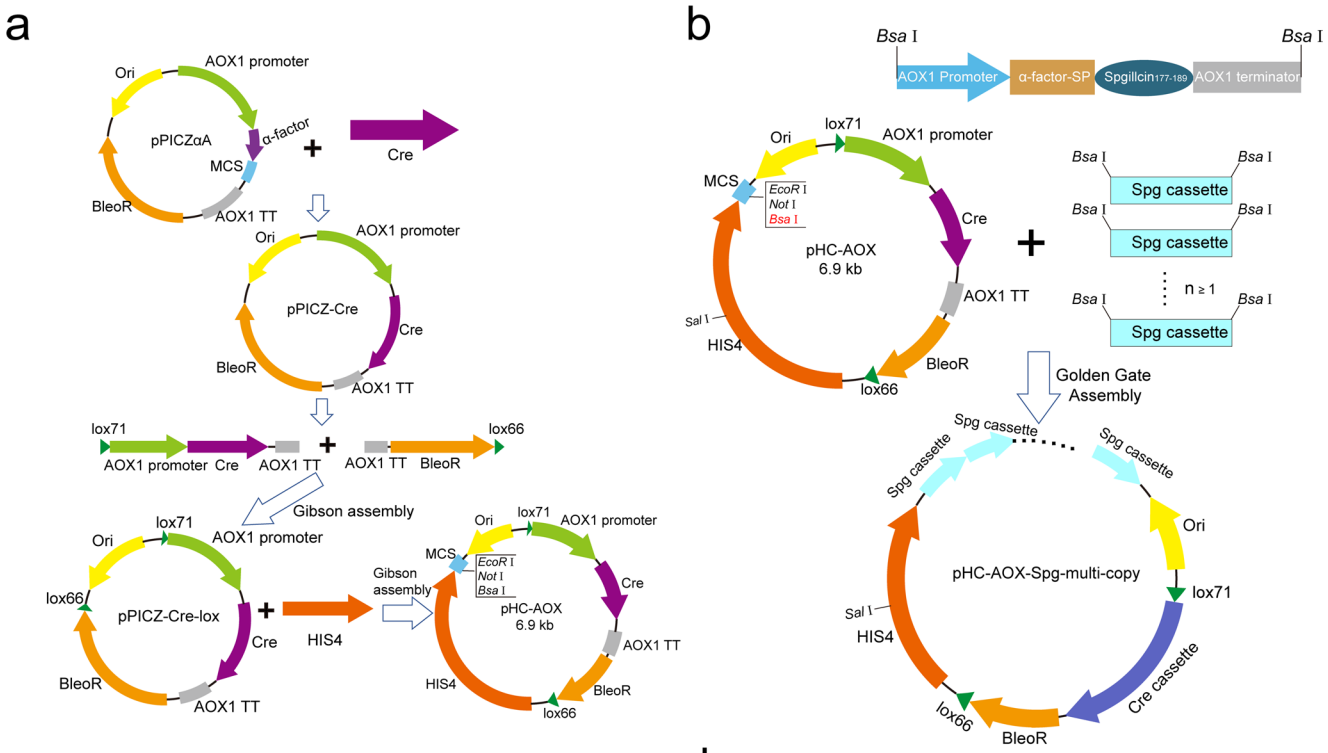
a
Ori
AOX1 promoter
pPICZαA
α-factor
MCS
BleoR
AOX1 TT
Cre
pPICZ-Cre
lox71
lox66
Gibson assembly
pPICZ-Cre-lox
HIS4
EcoR I
Not I
Bsa I
pHC-AOX
6.9 kb
Sal I
b
Bsa I
AOX1 Promoter
α-factor-SP
Spgillcin177-189
AOX1 terminator
Spg cassette
n ≥ 1
Golden Gate
Assembly
pHC-AOX-Spg-multi-copy
Cre cassette

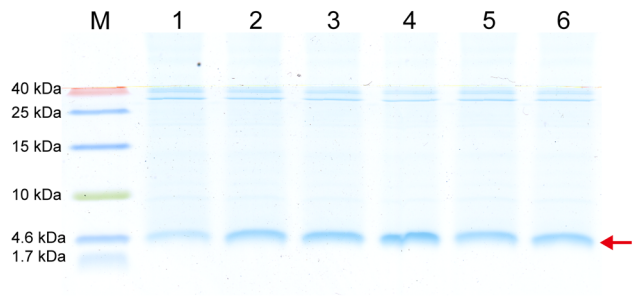
c
M
1
2
3
4
5
6
40 kDa
25 kDa
15 kDa
10 kDa
4.6 kDa
1.7 kDa

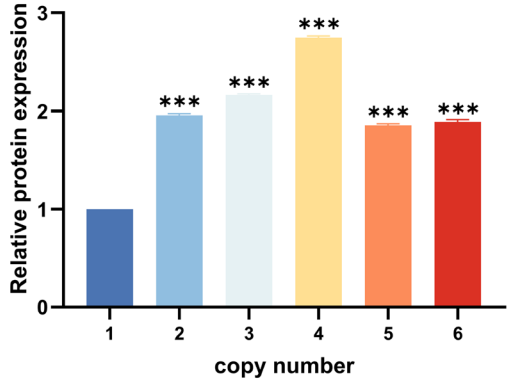
d
Relative protein expression
copy number
***

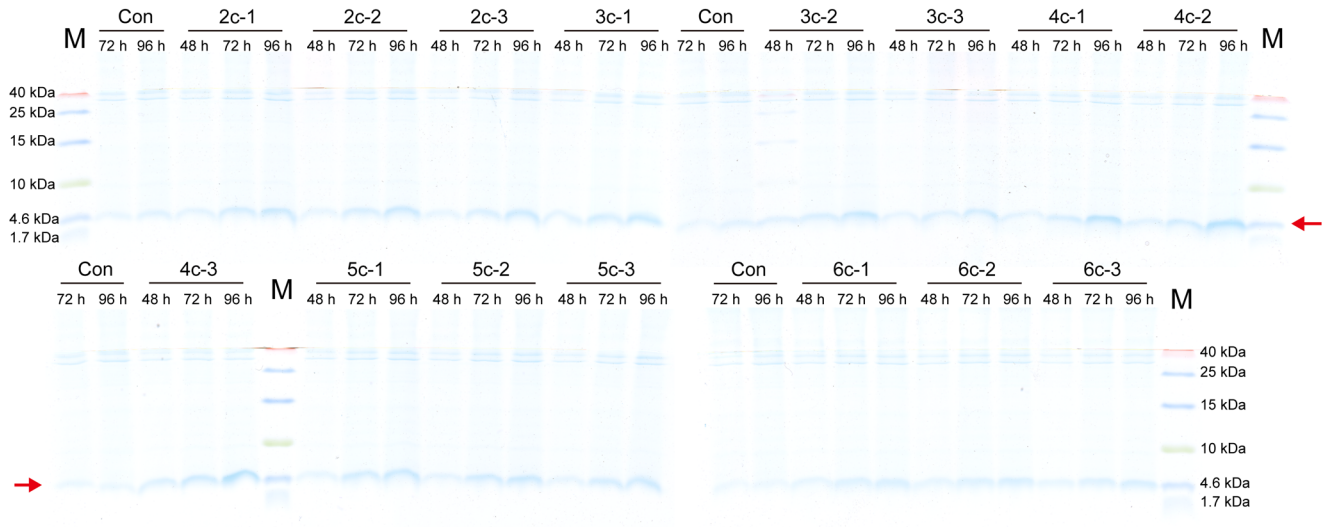
e
M
Con
2c-1
2c-2
2c-3
3c-1
3c-2
3c-3
4c-1
4c-2
4c-3
5c-1
5c-2
5c-3
6c-1
6c-2
6c-3
72 h
96 h
48 h
40 kDa
25 kDa
15 kDa
10 kDa
4.6 kDa
1.7 kDa

Fig. 2 Vector construction and recombinant proteins expression. (**a**) Schematic map of the construction of expression vector pHC. Ori: origin of replication, Cre: Causes recombination, MCS: Multiple Cloning Site, BleoR: Bleomycin Resistance, HIS4: Histidine Requirement 4. (**b**) Schematic map of the construction of the expression vectors pHC-spg with 1, 2,3, 4, 5, 6 copies of *Spg* gene. (**c**) Tricine-SDS-PAGE analysis at 96 h. Line 1–6: multicopy strains contained 1–6 copys of *Spg* gene. (**d**) The rSpgillcin$_{177-189}$ relative concentration was analyzed using image J software. Values are stated as mean ± SD (n = 3). (**e**) Tricine-SDS-PAGE analysis of rSpgillcin$_{177-189}$ in different strains at different times. Statistical significance is indicated by asterisks, *p < 0.05, **p < 0.01 and ***p < 0.001

compromised membranes. In the control group, nearly all bacteria exhibited green fluorescence, while treatment with rSpgillcin$_{177-189}$ markedly increased red fluorescence, indicating severe disruption of the cell membranes of *S. aureus* and *V. parahaemolyticus* (Fig. 6a, b).

Secondary Structure of rSpgillcin$_{177-189}$

The secondary structure of rSpgillcin$_{177–189}$ was analyzed using CD spectroscopy. As shown in Fig. 7b, the CD spectrum of rSpgillcin$_{177–189}$ dissolved in H_2O and 60 mM SDS exhibited a characteristic positive peak near 190 nm and two negative peaks at approximately 208 nm and 222 nm. The secondary structure composition of rSpgillcin$_{177–189}$ was estimated to be 36% α-helix, 17% β-sheet, and 47% random coil in H_2O, and 56% α-helix, 11% β-sheet, and 33% random coil in SDS, and 50% α-helix, 14% β-sheet, and 36% random coil in TFE. The increase in α-helical content under SDS and TFE conditions suggests that rSpgillcin$_{177–189}$ undergoes partial structural rearrangement in a membrane-mimicking environment, which may further enhance its affinity for bacterial membranes. This spectral result indicated that rSpgillcin$_{177-189}$ adopts a typical α-helical conformation, which is consistent with the predicted 3D model structure (Fig. 7a).

Effect of Exogenously Added Microbial Surface Components on the Antimicrobial Activity of rSpgillcin$_{177-189}$

Targeting membrane-associated molecules is a common antimicrobial mechanism for AMPs. The results showed that LPS and LTA significantly inhibited the antibacterial activity of rSpgillcin$_{177-189}$ in a dose-dependent manner. As shown in Fig. 7c & d, the antimicrobial activity of rSpgillcin$_{177-189}$ against *V. parahaemolyticus* and *S. aureus* decreased markedly with increasing concentrations of LTA or LPS.

Molecular Docking of rSpgillcin$_{177-189}$ with LPS and LTA

To investigate the interaction between rSpgillcin$_{177-189}$ and LPS/LTA, molecular docking analysis was performed to predict potential binding sites. As shown in Fig. 7e, rSpgillcin$_{177-189}$ formed two hydrogen bonds with LPS (ARG4–LIL803 and ARG8–GP42), with bond lengths of 2.4 Å and 2.6 Å, respectively. Additionally, three hydrogen bonds were observed at LYS2, ARG4, and ARG8 with LTA, with bond lengths of 1.9 Å, 3.2 Å, and 3.0 Å, respectively (Fig. 7f). These results suggest that hydrogen bonds may play a crucial role in the interaction between rSpgillcin$_{177-189}$ and LPS/LTA.

Stability Analysis of rSpgillcin$_{177-189}$

To evaluate the thermostability of rSpgillcin$_{177-189}$, we explored the effect of thermal treatment on the antimicrobial activity of rSpgillcin$_{177-189}$. The results showed that the bactericidal activity of rSpgillcin$_{177-189}$ against *S. aureus* and *V. parahaemolyticus* was retained after treated at different temperatures for 25 min (Fig. 8a, b). After heating at 100°C for 10 min, 20 min, and 30 min, the antimicrobial activity of rSpgillcin$_{177-189}$ against *S. aureus* and *V. parahaemolyticus* remained unchanged (Fig. 8c, d). These results indicated that rSpgillcin$_{177-189}$ had good thermostability.

Cytotoxicity and Hemolytic Activity of rSpgillcin$_{177-189}$

The cytotoxicity of rSpgillcin$_{177–189}$ was evaluated using HEK 293 T, RAW 264.7, and ZF4 cell lines. As shown in Fig. 8e-g, no significant cytotoxic effects were observed within the concentration range of 5.25–84 μg/mL. Moreover, rSpgillcin$_{177-189}$ exhibited negligible hemolytic activity against mouse erythrocytes (Fig. 8h). These findings demonstrate that rSpgillcin$_{177–189}$ possesses strong antibacterial activity while maintaining low cytotoxicity and hemolytic activity, highlighting its safety in organisms and its potential as a promising alternative to conventional antibiotics.

Discussion

Bacterial contamination caused by foodborne pathogens are a growing public health issue worldwide, posing a persistent challenge to human health. Alarmingly, in recent years, foodborne multi-drug resistant pathogens have been isolated from various food sources, indicating a potential risk of transmission to humans through contaminated food, which complicates the treatment of clinical infections [4]. Therefore, to develop new natural antibacterial agents to effectively control the spread of bacterial contamination and curb the emergence of antibiotic resistance is necessary. AMPs have received extensive attention as alternatives to

Table 1 The copy number analysis of multicopy strain

No.	Strains	Copy number of $Spgillcin_{177-189}$
1	GS115-pHC-Spg-1c	1.00
2	GS115-pHC-Spg-2c	1.91 ± 0.05
3	GS115-pHC-Spg-3c	2.78 ± 0.29
4	GS115-pHC-Spg-4c	3.83 ± 0.12
5	GS115-pHC-Spg-5c	4.68 ± 0.35
6	GS115-pHC-Spg-6c	5.58 ± 0.41

antibiotics [30]. Although AMPs hold immense potential as alternatives to antibiotics in both clinical medicine and livestock industries, their widespread application is hindered by manufacturing limitations. Although chemical synthesis enables small-scale AMP production for research, their high cost and poor scalability render it impractical for clinical or industrial use [8, 31].

Recombinant expression has emerged as a cost-effective approach for large-scale AMP production. However, conventional prokaryotic hosts like *E. coli* face intrinsic challenges, that is, the inherent toxicity of AMPs to bacterial cells and its susceptibility to proteolytic degradation often result in low yields [17, 32, 33]. In contrast, the eukaryotic yeast *P. pastoris* has distinct advantages. This expression platform not only enables efficient secretory production of AMPs, but also significantly reduces downstream purification costs through minimizing the secretion of endogenous host proteins [34].

Previous studies have demonstrated that $Spgillcin_{177-189}$ exhibits potent antibacterial activity against a broad spectrum of bacterial strains [7]. In this study, we aimed to improve the quantity of $rSpgillcin_{177-189}$ in *P. pastoris* expression system, thereby sufficiently meeting its application in industries. To achieve this, we optimized the codon usage of $Spgillcin_{177-189}$ and fused it to the α-factor signal peptide. In yeast cells, the α-factor signal peptide is specifically cleaved by signal peptidases, allowing for the production of $rSpgillcin_{177-189}$ with a native N-terminus. Moreover, previous studies have indicated that modifying the GC content and codon bias of target genes can enhance recombinant protein expression, likely due to transcriptional regulation [35].

Numerous studies have demonstrated that the multi-copy strategy is essential for improving protein expression [36]. Currently, two main approaches are employed for screening multi-copy strains, that is, in vivo random selection of high-copy strains and in vitro construction of multi-copy plasmids. The most commonly used in vivo method involves high-concentration antibiotic selection or the PTVA method [37], which rely on gradually increasing the concentration of antibiotics (e.g., Zeocin, G418) to randomly isolate high-copy strains. However, these methods are time-consuming and require one or more selectable markers. Given the limited availability of selectable markers in *P. pastoris*, this constraint may hinder subsequent selection of host cells [38]. To address this limitation, we developed a marker-free selection system based on the pPICZαA plasmid, drawing upon previous studies [38, 39]. Specifically, we introduced the lox71, lox66 sites and Cre recombinase cassette into the plasmid, positioning the resistance gene between the lox71 and lox66 sites. Following integration of the plasmid into the *P pastoris* genome, Cre recombinase was induced by methanol to excise lox71–resistance gene–lox66 fragment, thereby removing the resistance marker.

The in vitro construction of multi-copy plasmids is usually achieved using the isocaudamer (same-site restriction enzyme) method, which involves iterative rounds of digestion and ligation [21, 40]. Specifically, the target gene cassette is excised using dual-enzyme digestion (isocaudamer) and subsequently ligated into a linearized plasmid digested with a single restriction enzyme and dephosphorylated using alkaline phosphatase. This process increases the gene copy number from one to two, generating a 2-copy plasmid. Repeating this process allows the construction of multi-copy plasmids containing 4-copy or 8-copy cassettes. However, this method is cumbersome and time-consuming due to the requirement for multiple rounds of digestion and ligation. In this study, we employed the Golden Gate assembly technology to efficiently construct multi-copy plasmids. *Bsa* I, a type IIs restriction endonuclease, cleaves at sites different from its recognition sequence, enabling precise assembly of DNA fragments. This property facilitates the application of Golden Gate assembly to efficiently insert multiple expression cassettes into the *Bsa* I sites, allowing the generation of multi-copy recombinant plasmids. Unlike the isocaudamer method, the Golden Gate assembly method eliminates the need for multiple digestion-ligation steps. Instead, we designed primers incorporating distinct *Bsa* I recognition sites to amplify the target cassette, followed by a one-step Golden Gate reaction to assemble multiple cassettes ($n \geq 1$) in a single reaction, thereby generating plasmids with n copies ($n \geq 1$) of the target gene. This one-step method greatly reduces the time and labor required for multi-copy plasmid construction. Therefore, the pHC-AOX plasmid backbone offers a dual advantage: it enables the rapid assembly of multi-copy plasmids via Golden Gate cloning, while its Cre recombinase system facilitates the excision of the selection marker, enhancing its potential for commercial applications.

Subsequently, we successfully enhanced the expression level of rSpgillcin through the construction of multi-copy plasmid. This result is consistent with previous studies. For instance, the expression level of *Candida antarctica* lipase B was significantly enhanced using a multi-copy strategy, with the 3-copy strain yielding the highest production—2.3-fold higher than the single-copy strain [41]. Similarly, the yield of scFv variants was improved through multi-copy

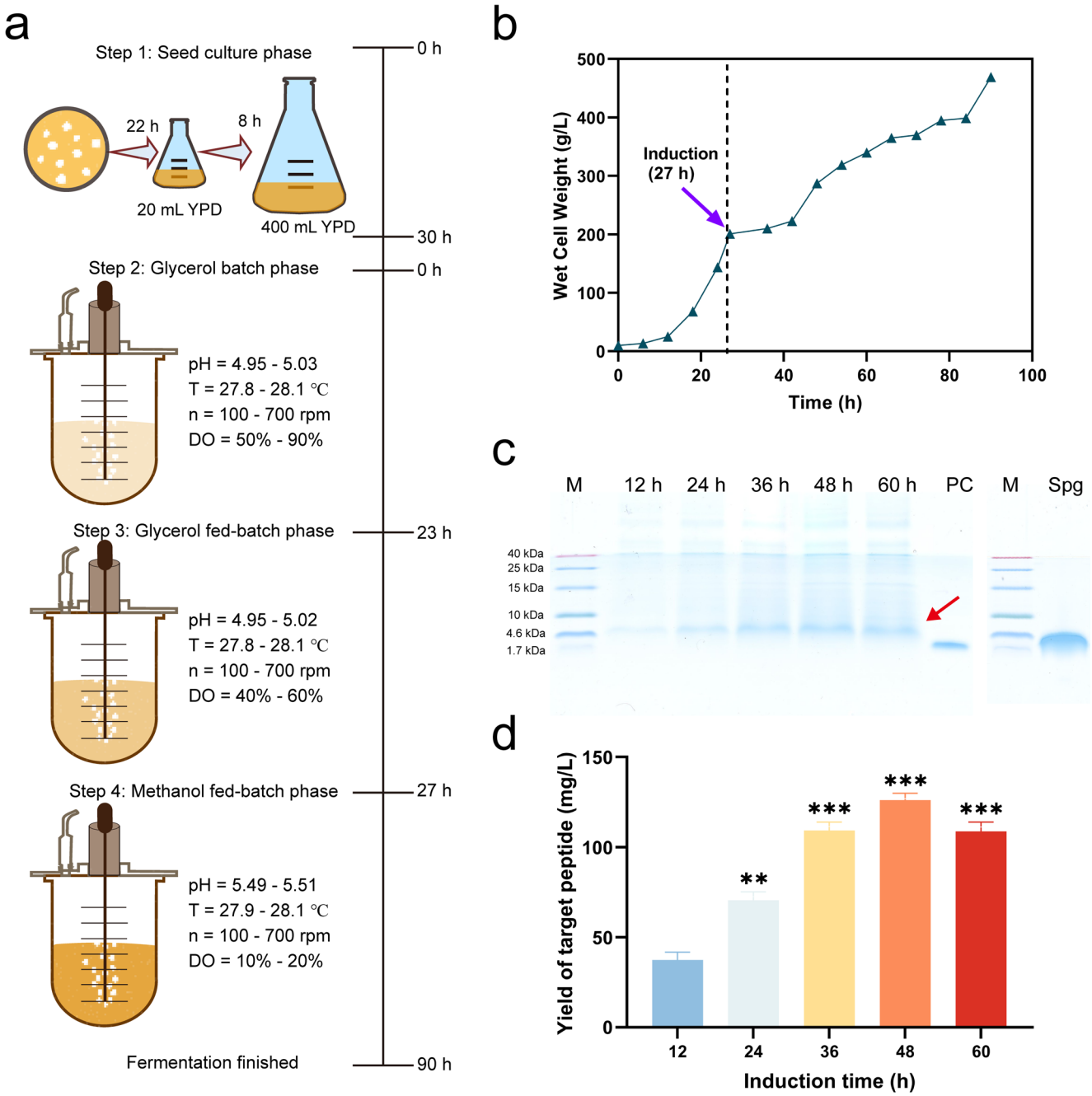

Fig. 3 High density fermentation of rSpgillcin$_{177-189}$. (**a**) Schematic diagram of high-density fermentation process. DO: Dissolved Oxygen, n: Agitation Speed, T: Temperature. (**b**) Cell growth curves of high-density induced fermentation. (**c**) Tricine-SDS-PAGE analysis. M: protein marker; 12–60 h: the fermentation supernatant of GS115-pHC-Spg-4c collected at different time points; PC: synthetic rSpgillcin$_{177-189}$ (1.5 ug); Spg: Purified rSpgillcin$_{177-189}$. (**d**) Concentration analysis of rSpgillcin$_{177-189}$ in the supernatant of fermentation broth. The rSpgillcin$_{177-189}$ concentration was analyzed using ImageJ software. Values are stated as mean ± SD ($n=3$). Statistical significance is indicated by asterisks, *$p<0.05$, **$p<0.01$ and ***$p<0.001$

integration, with the 6-copy strain showing the highest expression level [42]. Differently, the expression level of rSpgillcin$_{177-189}$ decreased in the 5-copy and 6-copy strains, which might be attributed to the metabolic burden on the translation and secretion pathways caused by excessive transcription [43, 44].

Large-scale production plays is essential for the industrial application of recombinant proteins, and protein yields from bioreactor fermentation are significantly higher than those from shake flasks [45]. In this study, the rSpgillcin$_{177-189}$ was expressed at a yield of 13.7 mg/L under shake flask conditions, demonstrating a favorable baseline expression level.

Table 3 Antimicrobial activity of rSpgillcin$_{177-189}$

Microorganisms	CGMCC No.	MIC (μg/mL)	MBC (μg/mL)
Gram-positive bacteria			
Bacillus cereus	1.3760	10.5–21	10.5–21
Listeria monocytogenes	1.10753	42–84	42–84
Staphylococcus epidermidis	1.4260	5.25–10.5	5.25–10.5
Staphylococcus aureus	1.2465	10.5–21	10.5–21
Gram-negative bacteria			
Acinetobacter baumannii	1.6769	10.5–21	10.5–21
Pseudomonas aeruginosa	1.2421	10.5–21	10.5–21
Vibrio fluvialis	1.1609	5.25–10.5	5.25–10.5
Vibrio harveyi	1.1593	10.5–21	10.5–21
Vibrio alginolyticus	1.1833	21–42	21–42
Vibrio parahaemolyticus	1.1615	21–42	21–42
Clinical isolates			
MRSA QZ19131	-	10.5–21	10.5–21
MRSA QZ19132	-	10.5–21	10.5–21
MDR *P. aeruginosa* QZ18071	-	21–42	21–42
MDR *P. aeruginosa* QZ18076	-	21–42	21–42

Several AMPs have previously been successfully expressed in *P. pastoris*. However, their production often faces limitations in yield and scalability. For instance, Turgencin A and human β-defensin 2 achieved a yield of 11.23 mg/L and 2 mg/L in shake flasks, respectively [46, 47]. While piscidin showed an expression level of 3.6 mg/L in shake flask, its yield dropped significantly to 0.8 mg/L in a 5 L bioreactor, indicating poor scalability and production stability [15]. In contrast, by employing high-density fermentation in a bioreactor, we achieved a maximum yield of 126.1 mg/L for rSpgillcin$_{177-189}$, demonstrating a significant advantage in both production level and scalability. Subsequently, rSpgillcin$_{177-189}$ was purified using cation exchange chromatography to obtain a high-purity recombinant peptide, which was used for further investigation of its antimicrobial activity and mechanism.

In the present study, the results confirmed that the antimicrobial activity of rSpgillcin$_{177-189}$ against clinical MDR strains was comparable to that of chemically synthesized Spgillcin$_{177-189}$. Moreover, we also discovered that rSpgillcin$_{177-189}$ exhibits strong antibacterial activity against

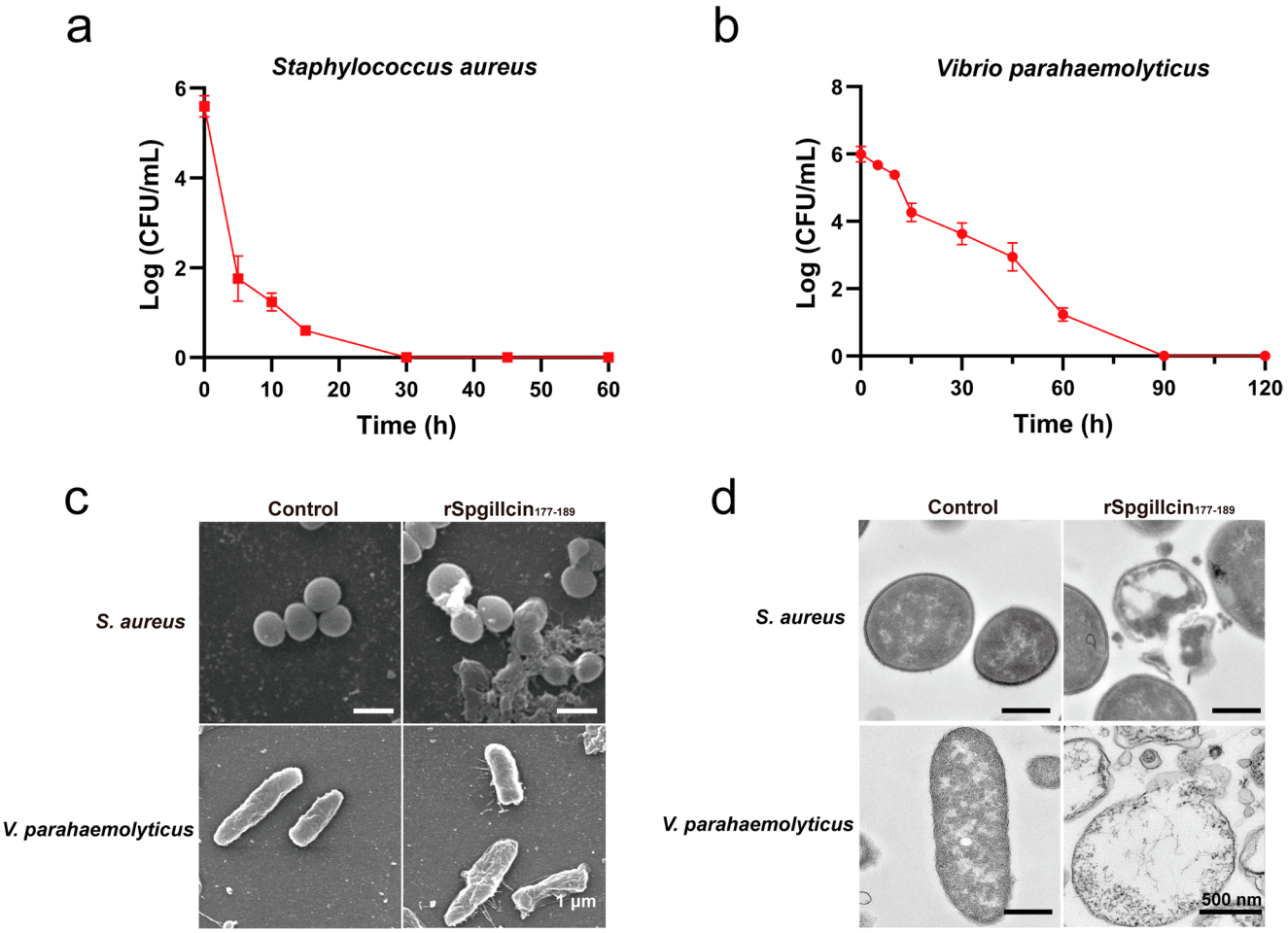

Fig. 4 Time-killing kinetic curves of rSpgillcin$_{177-189}$ on *S. aureus* (**a**) and *V. parahaemolyticus* (**b**). Effect of rSpgillcin$_{177-189}$ on morphological and structural changes of *S. aureus* and *V. Parahaemolyticus* observed by SEM (**c**) and TEM (**d**)

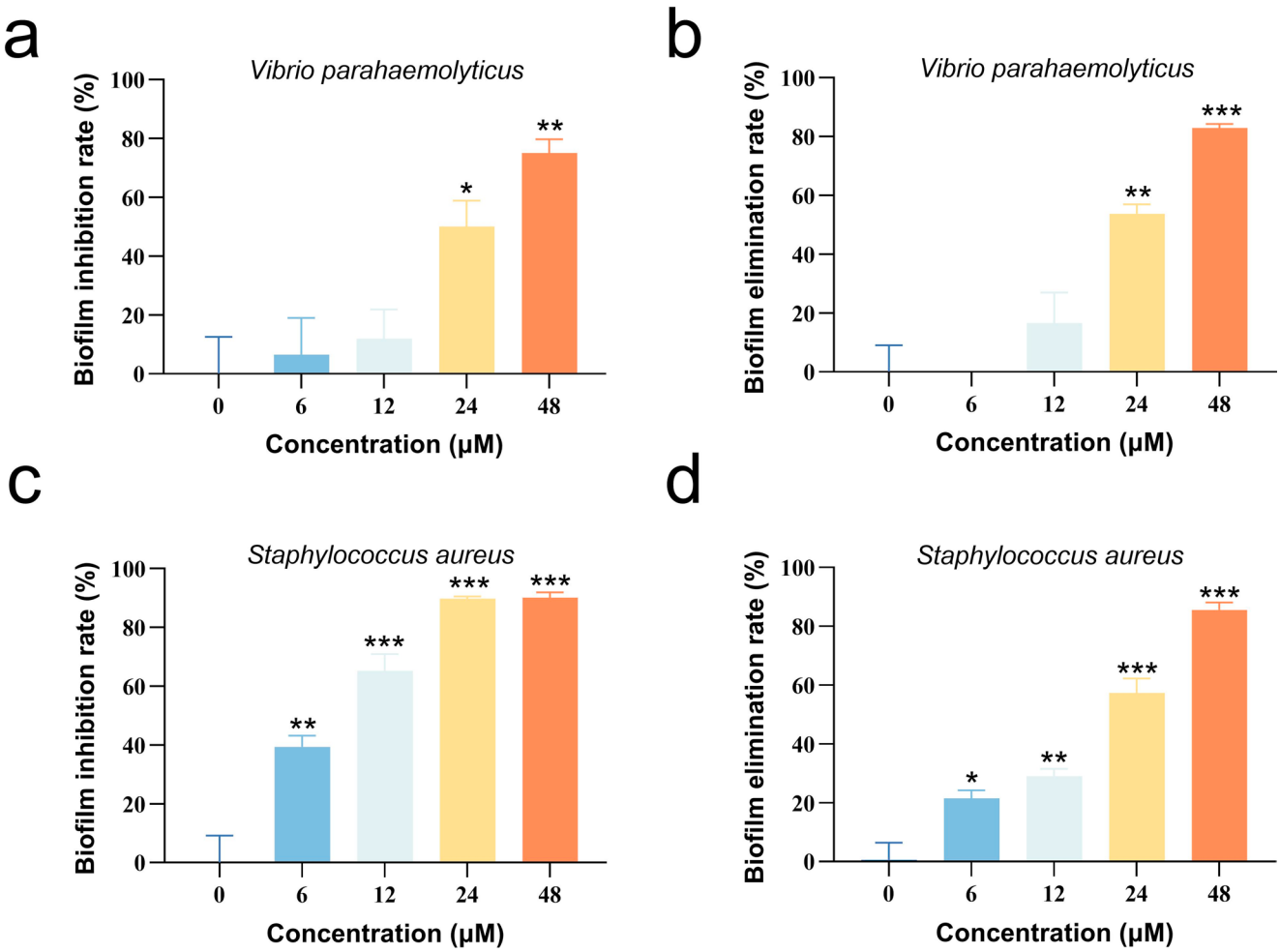

Fig. 5 The inhibitory effects of rSpgillcin$_{177-189}$ on *V. parahaemolyticus* (**a**), *S. aureus* (**b**) biofilm formation. The elimination effects *V. parahaemolyticus* (**b**) and *S. aureus* (**d**) mature biofilm. Statistical significance is indicated by asterisks, *$p<0.05$, **$p<0.01$ and ***$p<0.001$

foodborne pathogens. Biofilms are extracellular polymeric structures that exhibit far greater resistance to antibiotics compared with planktonic cells. In addition, biofilms can adhere to medical devices and host tissues, accounting for nearly 80% of hospital-acquired infections [48]. Our results demonstrated that rSpgillcin$_{177-189}$ not only effectively inhibited biofilm formation but also exhibited pronounced activity in disrupting mature biofilms. Furthermore, SEM, TEM, and SYTO9/PI assays revealed that the antibacterial mechanism of rSpgillcin$_{177-189}$ involved disruption of bacterial membrane integrity, resulting in leakage of intracellular contents and ultimately causing cell death. Consistently, LPS-binding assays further supported this mechanism, suggesting that rSpgillcin$_{177-189}$ may exert its bactericidal effect through interactions with the bacterial cell membrane. In addition, rSpgillcin177–189 showed no cytotoxicity toward vertebrate cell lines and exhibited negligible hemolytic activity against mouse erythrocytes, indicating excellent biocompatibility and suggesting that its application in vivo would be both safe and effective. Taken together, these findings demonstrate that the recombinant peptide rSpgillcin$_{177–189}$ possesses strong antimicrobial activity and functional stability, while offering a more economical production process with enhanced peptide yield. This study highlights the potential of rSpgillcin$_{177–189}$ for industrial applications in medicine and the food industry.

Furthermore, to achieve a deeper insight into the relationship between structure and function of AMPs, we employed bioinformatics approaches to predict the 3D structure of rSpgillcin$_{177-189}$ and analyzed its secondary structure using CD. The results demonstrated that rSpgillcin$_{177-189}$ adopts a typical α-helical conformation consistent with most AMPs, like AMP KTA, AW1 and Larimicin$_{78-102}$ [49–51], thereby validating the reliability of the structural prediction (Fig. 7a). The amphipathic α-helix conformation allows AMPs to interact with lipid head regions of microbial membranes, insert into the bilayer, and form transmembrane pores, ultimately resulting in cell lysis and death [52].

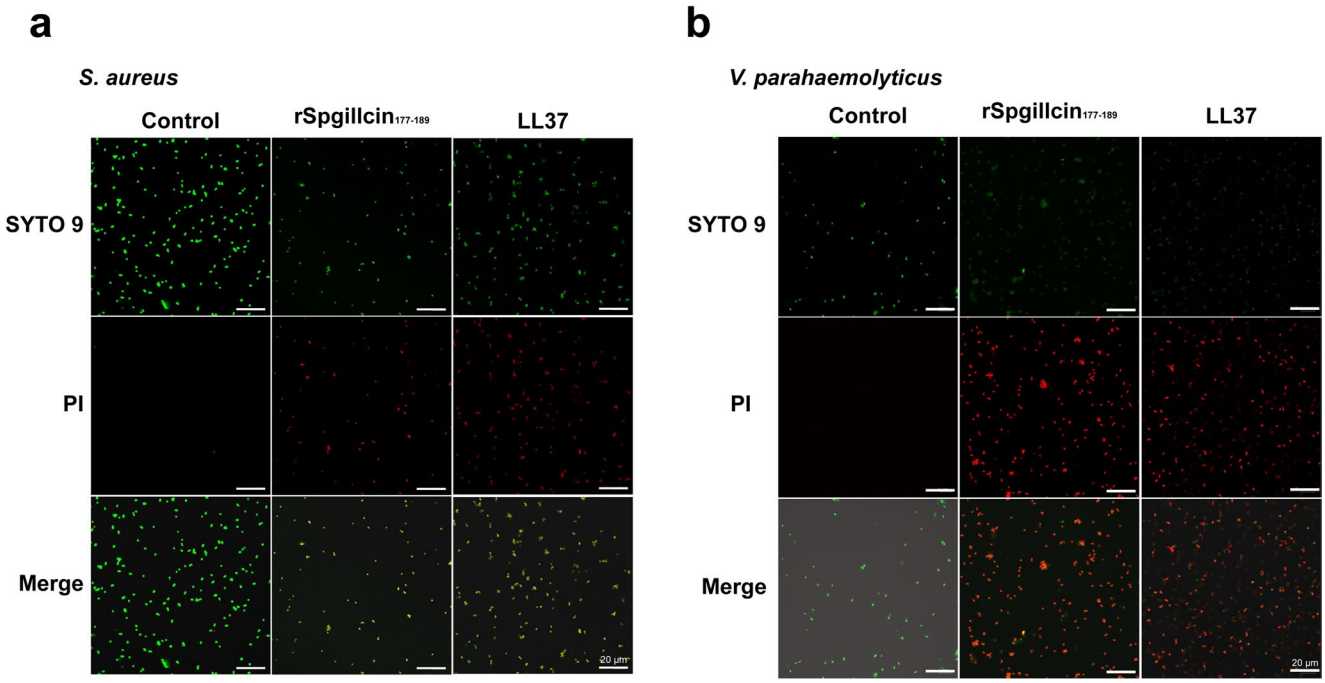

Fig. 6 Effect of rSpgillcin$_{177-189}$ on membrane permeability of *S. aureus* (**a**) and *V. parahaemolyticus* (**b**). CLSM images illustrating bacterial membrane permeability assessed by SYTO9/PI staining following treatment with rSpgillcin$_{177-189}$

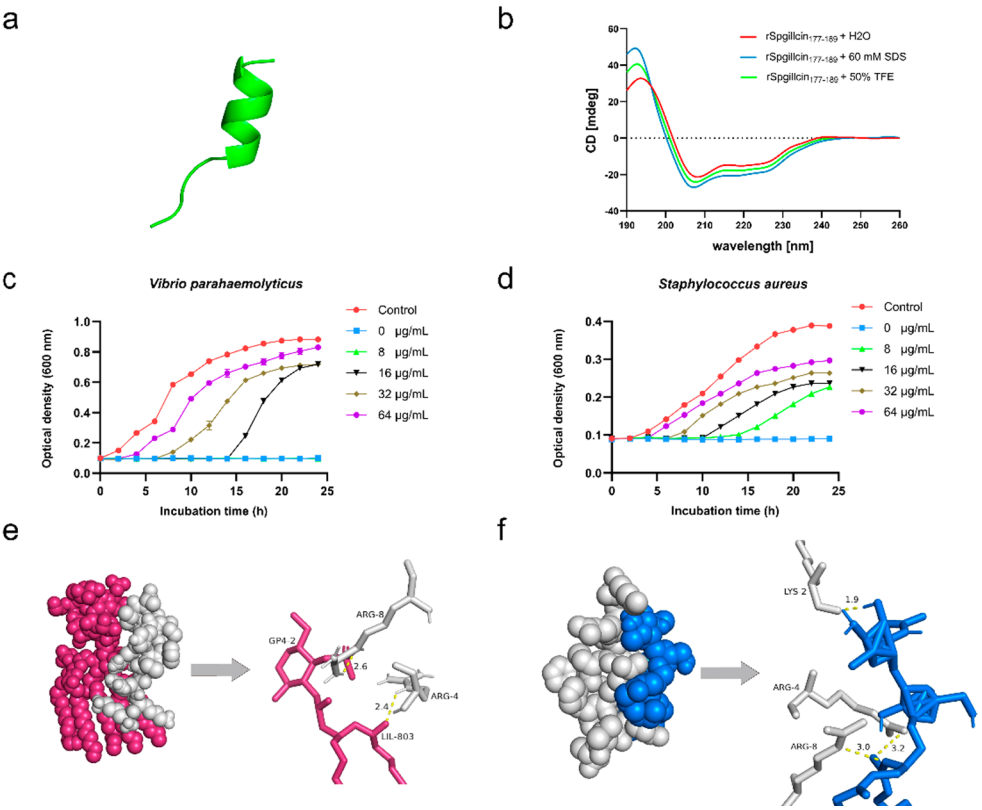

Fig. 7 The 3D model (**a**) and secondary structure (**b**) rSpgillcin$_{177-189}$. Effect of exogenous LPS and LTA on rSpgillcin$_{177-18}$ against *V. Parahaemolyticus* (**c**) and *S. aureus* (**d**). Interaction between peptides and LPS (**e**) & LTA (f). rSpgillcin$_{177-189}$ is shown as grey. LPS and LTA are shown as red and blue, respectively. The hydrogen bonds are shown in yellow dotted lines

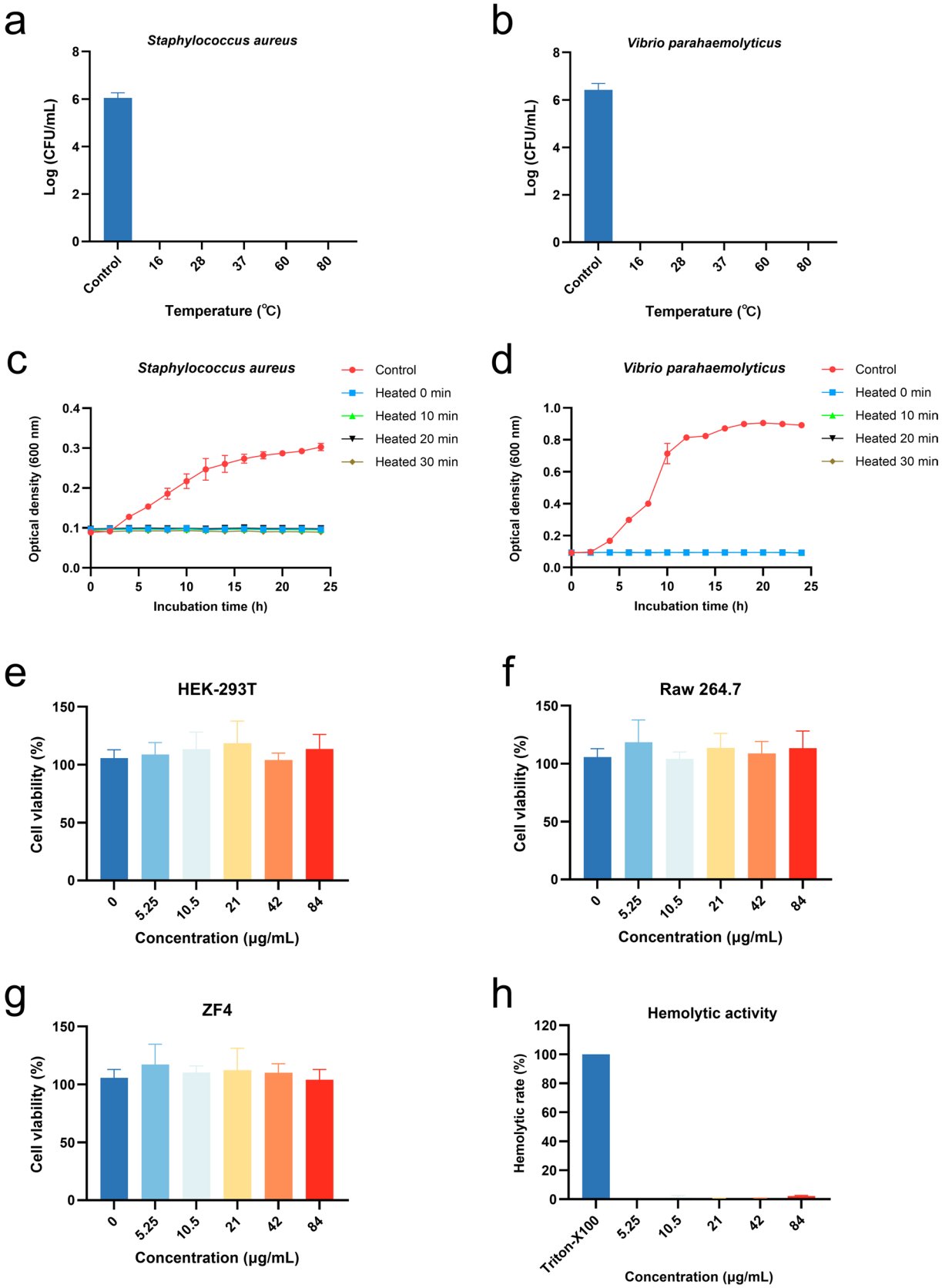

Fig. 8 Thermostability evaluation of rSpgillcin$_{177-189}$. *S. aureus* (**a**, **c**) and *V. Parahaemolyticus* (**b**, **d**) were treated with heated rSpgillcin$_{177-189}$. The cytotoxicity of rSpgillcin$_{177-189}$ on HEK-293T (**e**), RAW264.7 (**f**), ZF4 (**g**) cell lines. Hemolytic activity of rSpgillcin$_{177-18}$ on mouse erythrocytes (**h**)

Microbial cell surfaces are enriched with phospholipids, which impart a net negative charge [53, 54]. Specifically, Gram-positive bacteria contain LTA, whereas Gram-negative bacteria possess LPS, both of which are strongly negatively charged and serve as the main targets of AMPs. For instance, AMP epifensin-1 interacted with negatively charged bacterial membrane components through electrostatic interactions, leading to membrane disruption, and bacterial cell death [55]. The results indicate that the exogenous addition of LPS and LTA reduces the antimicrobial activity of rSpgillcin$_{177-189}$. These findings suggest that rSpgillcin$_{177-189}$ may exert its bactericidal effects by binding to LTA and LPS on the surfaces of bacteria, respectively.

To further investigate the potential interactions between rSpgillcin$_{177-189}$ and LPS/LTA, we conducted molecular docking analysis to identify potential binding sites. The results revealed that rSpgillcin$_{177-189}$ forms multiple hydrogen bonds with LPS and LTA, exhibiting high binding affinity. These findings suggest that rSpgillcin$_{177-189}$ may not only rely on electrostatic interactions, but also form hydrogen bonds with LTA and LPS, ultimately altering membrane permeability and leading to cell death. These hydrogen bond-forming residues may represent critical sites influencing the antimicrobial activity of rSpgillcin$_{177-189}$, and mutations at these positions may alter its bactericidal efficacy. It has been reported that sequence mutations or domain insertions in AMPs can affect their affinity for LPS, as observed with AMP L7 [24].

Conclusion

In summary, this study successfully produced the AMP rSpgillcin$_{177-189}$ in *P. pastoris*, and the yield of rSpgillcin$_{177-189}$ was significantly enhanced using a multicopy strategy. Subsequently, high-density fermentation was performed in a bioreactor to achieve large-scale production, and the antimicrobial activity of rSpgillcin$_{177-189}$ against both clinical MDR strains and foodborne pathogens was validated. rSpgillcin$_{177-189}$ showed good thermostability and no obvious cytotoxicity and hemolytic activity. Furthermore, rSpgillcin$_{177-189}$ may interact with microbial surface components via hydrogen bonding, specifically targeting the cell membranes of *S. aureus* and *V. parahaemolyticus*, leading to increase membrane permeability and bacterial cell death. Overall, this study provides a potential solution for the industrial-scale production of rSpgillcin$_{177-189}$ and establishes a foundation for its application in biomedical and food industries. In future work, it is worthy to further optimize key production parameters to enhance the scalability and cost-effectiveness of rSpgillcin$_{177-189}$, and systematically evaluate its application potential as a food preservation in various matrices, to facilitate its industrial translation.

Supplementary Information The online version contains supplementary material available at https://doi.org/10.1007/s12602-025-10874-y.

Acknowledgements We also express our gratitude to laboratory engineers Zhiyong Lin, Huiyun Chen for their technical assistance throughout the study.

Author Contributions Xx. D: Writing – original draft, Investigation, Methodology, Formal analysis, Data curation. Hl. L: Methodology, Investigation. H.P: Methodology, Investigation. C.Z: Methodology, Investigation. X.H: Investigation. H.H: Methodology. M.X: Methodology. Jh.M: Investigation. Fy.C: Writing – review & editing, Supervision, Supervision, Funding acquisition, Conceptualization. Kj.W: Writing – review & editing, Project administration, Funding acquisition, Conceptualization.

Data Availability No datasets were generated or analysed during the current study.

Declarations

Competing Interests The authors declare no competing interests.

References

1. Zhang XH, Guo MM, Ismail BB et al (2021) Informative and corrective responsive packaging: advances in farm-to-fork monitoring and remediation of food quality and safety. [Review]. Compr Rev Food Sci Food Saf 20(5):5258–5282. https://doi.org/10.1111/1541-4337.12807
2. Burden of Foodborne Illnesses in the United States (2025) https://www.cdc.gov/food-safety/php/data-research/foodborne-illness-burden/?CDC_AAref_Val=https://www.cdc.gov/foodbornenburden/burden/index.html
3. Nadeem SF, Gohar UF, Tahir SF et al (2020) Antimicrobial resistance: more than 70 years of war between humans and bacteria. Crit Rev Microbiol 46(5):578–599. https://doi.org/10.1080/1040841X.2020.1813687
4. Friedman M (2015) Antibiotic-resistant bacteria: prevalence in food and inactivation by food-compatible compounds and plant extracts. J Agric Food Chem 63(15):3805–3822. https://doi.org/10.1021/acs.jafc.5b00778
5. Goldberg K, Lobov A, Antonello P et al (2025) Cell-autonomous innate immunity by proteasome-derived defence peptides. Nature 639(8056):1032–1041. https://doi.org/10.1038/s41586-025-08615-w
6. Zhang C, Chen F, Bai Y et al (2024) A novel antimicrobial peptide Spasin141-165 identified from *Scylla paramamosain* exhibiting protection against *Aeromonas hydrophila* infection. Aquaculture 741137. https://doi.org/10.1016/j.aquaculture.2024.741137
7. Wang X, Hong X, Chen F, Wang K-J (2022) A truncated peptide Spgillcin177–189 derived from mud crab scylla paramamosain exerting multiple antibacterial activities. Front Cell Infect Microbiol 12:928220. https://doi.org/10.3389/fcimb.2022.928220
8. Chaudhary S, Ali Z, Tehseen M et al (2023) Efficient in planta production of amidated antimicrobial peptides that are active against drug-resistant ESKAPE pathogens. Nat Commun 14(1):1464. https://doi.org/10.1038/s41467-023-37003-z
9. Parachin NS, Mulder KC, Viana AAB et al (2012) Expression systems for heterologous production of antimicrobial peptides. Peptides 38(2):446–456. https://doi.org/10.1016/j.peptides.2012.09.020

10. Kesidis A, Depping P, Lodé A et al (2020) Expression of eukaryotic membrane proteins in eukaryotic and prokaryotic hosts. Methods 180:3–18. https://doi.org/10.1016/j.ymeth.2020.06.006
11. Deo S, Turton KL, Kainth T et al (2022) Strategies for improving antimicrobial peptide production. Biotechnol Adv 59:107968. https://doi.org/10.1016/j.biotechadv.2022.107968
12. Bommarius B, Jenssen H, Elliott M et al (2010) Cost-effective expression and purification of antimicrobial and host defense peptides in *Escherichia coli*. Peptides 31(11):1957–1965. https://doi.org/10.1016/j.peptides.2010.08.008
13. Karbalaei M, Rezaee SA, Farsiani H (2020) *Pichia pastoris*: a highly successful expression system for optimal synthesis of heterologous proteins. J Cell Physiol 235(9):5867–5881. https://doi.org/10.1002/jcp.29583
14. Daly R, Hearn MT (2005) Expression of heterologous proteins in *Pichia pastoris*: a useful experimental tool in protein engineering and production. J Mol Recognit 18(2):119–138. https://doi.org/10.1002/jmr.687
15. Tai H, Huang H, Tsai T et al (2020) Dietary supplementation of recombinant antimicrobial peptide *Epinephelus lanceolatus* piscidin improves growth performance and immune response in *Gallus gallus domesticus*. PLoS One 15(3):e0230021. https://doi.org/10.1371/journal.pone.0230021
16. Tai H, You M, Lin C et al (2021) Scale-up production of and dietary supplementation with the recombinant antimicrobial peptide tilapia piscidin 4 to improve growth performance in *Gallus gallus domesticus*. PLoS One 16(6):e0253661. https://doi.org/10.1371/journal.pone.0253661
17. Zhao L, Li L, Hu M et al (2024) Heterologous expression of the novel dimeric antimicrobial peptide LIG in *Pichia pastoris*. J Biotechnol 381:19–26. https://doi.org/10.1016/j.jbiotec.2023.12.015
18. Yang Z, Zhang Z (2017) Codon-optimized expression and characterization of a pH stable fungal xylanase in *Pichia pastoris*. Process Biochem 53:80–87. https://doi.org/10.1016/j.procbio.2016.11.022
19. Li C, Lin Y, Zheng X et al (2015) Combined strategies for improving expression of *citrobacter amalonaticus* phytase in *Pichia pastoris*. BMC Biotechnol 15:1–11. https://doi.org/10.1186/s12896-015-0204-2
20. Ata Ö, Prielhofer R, Gasser B et al (2017) Transcriptional engineering of the glyceraldehyde-3-phosphate dehydrogenase promoter for improved heterologous protein production in *Pichia pastoris*. Biotechnol Bioeng 114(10):2319–2327. https://doi.org/10.1002/bit.26363
21. Yang J, Lu Z, Chen J et al (2016) Effect of cooperation of chaperones and gene dosage on the expression of Porcine PGLYRP-1 in *Pichia pastoris*. Appl Microbiol Biotechnol 100(12):5453–5465. https://doi.org/10.1007/s00253-016-7372-4
22. Bai Y, Zhang W, Zheng W et al (2024) A 14-amino acid cationic peptide Bolespleenin334-347 from the marine fish mudskipper *Boleophthalmus pectinirostris* exhibiting potent antimicrobial activity and therapeutic potential. Biochem Pharmacol 116344. https://doi.org/10.1016/j.bcp.2024.116344
23. Zhang W, An Z, Bai Y et al (2023) A novel antimicrobial peptide Scyreptin1-30 from *Scylla paramamosain* exhibiting potential therapy of *Pseudomonas aeruginosa* early infection in a mouse burn wound model. Biochem Pharmacol 218:115917. https://doi.org/10.1016/j.bcp.2023.115917
24. Wang Z, Teng D, Mao R et al (2023) A cleavable chimeric peptide with targeting and killing domains enhances LPS neutralization and antibacterial properties against multi-drug resistant *E. coli*. Commun Biol 6(1):1170. https://doi.org/10.1038/s42003-023-05528-0
25. Jiang M, Chen R, Zhang J et al (2022) A novel antimicrobial peptide spampcin56–86 from *Scylla paramamosain* exerting rapid bactericidal and anti-biofilm activity in vitro and anti-infection in vivo. Int J Mol Sci 23(21):13316. https://doi.org/10.3390/ijms232113316
26. Xue B, Li Y-Y, Zheng B-F-C et al (2025) Expression and characterization of Recombinant triple laterosporulin in chlamydomonas reinhardtii. Probiotics Antimicrob Proteins. https://doi.org/10.1007/s12602-025-10523-4
27. Wang J, Song J, Yang Z et al (2019) Antimicrobial peptides with high proteolytic resistance for combating Gram-Negative bacteria. J Med Chem 62(5):2286–2304. https://doi.org/10.1021/acs.jmedchem.8b01348
28. Shi Y, Mowery RA, Ashley J et al (2012) Abnormal SDS-PAGE migration of cytosolic proteins can identify domains and mechanisms that control surfactant binding. Protein Sci 21(8):1197–1209. https://doi.org/10.1002/pro.2107
29. Walkenhorst WF, Merzlyakov M, Hristova K, Wimley WC (2009) Polar residues in transmembrane helices can decrease electrophoretic mobility in polyacrylamide gels without causing helix dimerization. Biochim Et Biophys Acta (BBA) - Biomembr 1788(6):1321–1331. https://doi.org/10.1016/j.bbamem.2009.02.017
30. Chen Y-C, Yang Y, Zhang C et al (2021) A novel antimicrobial peptide Sparamosin26–54 from the mud crab *scylla paramamosain* showing potent antifungal activity against *Cryptococcus neoformans*. Front Microbiol 12:746006. https://doi.org/10.3389/fmicb.2021.746006
31. Cao J, de la Fuente-Nunez C, Ou RW et al (2018) Yeast-based synthetic biology platform for antimicrobial peptide production. ACS Synth Biol 7(3):896–902. https://doi.org/10.1021/acssynbio.7b00396
32. Zhao L, Li L, Xu Y et al (2024) Heterologous expression and activity of α-helical antimicrobial peptide SW in *Bacillus subtilis*. Biochem. Eng. J. 203:109224. https://doi.org/10.1016/j.bej.2024.109224
33. Nana Z, Tai A, Yuan Z et al (2024) Improving photocleavage efficiency of photocleavable protein for antimicrobial peptide Histatin 1 expression. Protein Pept Lett 31(2):141–152. https://doi.org/10.2174/0109298665276722231212053009
34. Ahmad M, Hirz M, Pichler H, Schwab H (2014) Protein expression in *Pichia pastoris*: recent achievements and perspectives for heterologous protein production. Appl Microbiol Biotechnol 98:5301–5317. https://doi.org/10.1007/s00253-014-5732-5
35. Elena C, Ravasi P, Castelli ME et al (2014) Expression of codon optimized genes in microbial systems: current industrial applications and perspectives. Front Microbiol 5:21. https://doi.org/10.3389/fmicb.2014.00021
36. Damasceno LM, Huang C-J, Batt CA (2012) Protein secretion in *Pichia pastoris* and advances in protein production. Appl Microbiol Biotechnol 93:31–39. https://doi.org/10.1007/s00253-011-3654-z
37. Aw R, Polizzi KM (2016) Liquid PTVA: a faster and cheaper alternative for generating multi-copy clones in *Pichia pastoris*. Microb Cell Fact 15:1–11. https://doi.org/10.1186/s12934-016-0432-8
38. Pan R, Zhang J, Shen W-L et al (2011) Sequential deletion of *Pichia pastoris* genes by a self-excisable cassette. FEMS Yeast Res 11(3):292–298. https://doi.org/10.1111/j.1567-1364.2011.00716.x
39. Li D, Zhang B, Li S et al (2017) A novel vector for construction of markerless multicopy overexpression transformants in *Pichia pastoris*. Front Microbiol 8:1698. https://doi.org/10.3389/fmicb.2017.01698
40. Zhu T, Guo M, Tang Z et al (2009) Efficient generation of multi-copy strains for optimizing secretory expression of porcine insulin precursor in yeast *Pichia pastoris*. J Appl Microbiol 107(3):954–963. https://doi.org/10.1111/j.1365-2672.2009.04279.x

41. Robert JM, Betancur MO, Machado ACO et al (2019) Increase of *Candida Antarctica* lipase B production under PGK promoter in *Pichia pastoris*: effect of multicopies. Braz J Microbiol 50:405–413. https://doi.org/10.1007/s42770-019-00056-8
42. Wang N, Xiao Y, Liu X et al (2025) Structural homology fails to predict secretion efficiency in *Pichia pastoris*: divergent responses of architecturally similar scFvs to multi-parametric genetic engineering. Int J Mol Sci 26(10):4922. https://doi.org/10.3390/ijms26104922
43. Malhotra JD, Kaufman RJ (2007) The endoplasmic reticulum and the unfolded protein response. Semin Cell Dev Biol 18(6):716–731. https://doi.org/10.1016/j.semcdb.2007.09.003
44. Aw R, Polizzi KM (2013) Can too many copies spoil the broth? Microb Cell Fact 12:1–9. https://doi.org/10.1186/1475-2859-12-128
45. Yang Z, Zhang Z (2018) Engineering strategies for enhanced production of protein and bio-products in *Pichia pastoris*: a review. Biotechnol Adv 36(1):182–195. https://doi.org/10.1016/j.biotechadv.2017.11.002
46. Dong C, Li M, Zhang R et al (2023) The expression of antibacterial peptide Turgencin A in *Pichia pastoris* and an analysis of its antibacterial activity. Molecules 28(14):5405. https://doi.org/10.3390/molecules28145405
47. Çobanoğlu Ş, Arslan E, Yazıcı A, Örtücü S (2023) Expression of human β-defensin 2 (hBD-2) in *Pichia pastoris* and investigation of its binding efficiency with ACE-2. Protein J 42(4):399–407. https://doi.org/10.1007/s10930-023-10130-8
48. Zhang M-Y, Li S, Han Y-L et al (2025) De novo-designed amphiphilic α-helical peptide Z2 exhibits broad-spectrum antimicrobial, anti-biofilm, and anti-inflammatory efficacy in acute *Pseudomonas aeruginosa* pneumonia. Bioorg Chem 157:108309. https://doi.org/10.1016/j.bioorg.2025.108309
49. Zhang X, Ma P, Ismail BB et al (2024) Chickpea-derived modified antimicrobial peptides KTA and KTR inactivate *Staphylococcus aureus* via disrupting cell membrane and interfering with peptidoglycan synthesis. J Agric Food Chem 72(5):2727–2740. https://doi.org/10.1021/acs.jafc.3c08241
50. Ye Z, Fu L, Li S et al (2024) Synergistic collaboration between AMPs and non-direct antimicrobial cationic peptides. Nat Commun 15(1):7319. https://doi.org/10.1038/s41467-024-51730-x
51. Zhou Z, Chen F, Hao H, Wang K-j (2025) A novel antimicrobial peptide Larimicin78-102 from large yellow croaker (*Larimichthys crocea*) shows potent antibacterial activity in vitro and enhances resistance to vibrio fluvialis infection in vivo. Fish Shellfish Immunol 161:110279. https://doi.org/10.1016/j.fsi.2025.110279
52. Chen Y, Cai S, Qiao X et al (2017) As-CATH1–6, novel cathelicidins with potent antimicrobial and immunomodulatory properties from *Alligator sinensis*, play pivotal roles in host antimicrobial immune responses. Biochem J 474(16):2861–2885. https://doi.org/10.1042/BCJ20170334
53. Xhindoli D, Pacor S, Benincasa M et al (2016) The human cathelicidin LL-37—a pore-forming antibacterial peptide and host-cell modulator. Biochimica et Biophysica Acta (BBA) - Biomembranes 1858(3):546–566. https://doi.org/10.1016/j.bbamem.2015.11.003
54. Ma L, Wang Y, Wang M et al (2016) Effective antimicrobial activity of Cbf-14, derived from a cathelin-like domain, against penicillin-resistant bacteria. Biomaterials 87:32–45. https://doi.org/10.1016/j.biomaterials.2016.02.011
55. Narayana JL, Huang H-N, Wu C-J, Chen J-Y (2015) Epinecidin-1 antimicrobial activity: in vitro membrane lysis and in vivo efficacy against *Helicobacter pylori* infection in a mouse model. Biomaterials 61:41–51. https://doi.org/10.1016/j.biomaterials.2015.05.014

Publisher's Note Springer Nature remains neutral with regard to jurisdictional claims in published maps and institutional affiliations.

Springer Nature or its licensor (e.g. a society or other partner) holds exclusive rights to this article under a publishing agreement with the author(s) or other rightsholder(s); author self-archiving of the accepted manuscript version of this article is solely governed by the terms of such publishing agreement and applicable law.